Biogenic Hydroxyapatite Obtained from Bone Wastes Using CO_2-Assisted Pyrolysis and Its Interaction with Glyphosate: A Computational and Experimental Study

Diego F. Hernández-Barreto, Heriberto Hernández-Cocoletzi, and Juan Carlos Moreno-Piraján*

ACCESS | Metrics & More | Article Recommendations | SI Supporting Information

ABSTRACT: In this work, biogenic hydroxyapatite (BHap) obtained from cattle bone waste is proposed as an adsorbent of this dangerous pollutant. Density functional theory (DFT) and calorimetric studies were developed to study the interaction between BHap and glyphosate (GLY). A strong interaction was found in the experiments through the measurement of immersion enthalpy, confirmed by the exothermic chemisorption obtained with DFT calculations. These results suggest that hydroxyapatite is a promising adsorbent material for GLY adsorption in aqueous solutions. In addition, it was determined that the GLY−hydroxyapatite interaction is greater than the water−hydroxyapatite interaction, which favors the GLY adsorption into this material.
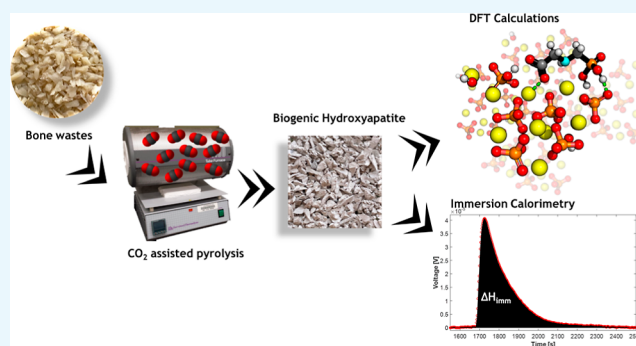
1. INTRODUCTION

Agricultural industry is one of the most important industries since it has made a major contribution to worldwide development. Meeting the global demand caused by the rapid population growth is one of the sustainable challenges faced by this industry as well as the efficient management of waste and residue.[1] Innovation and technological development of agriculture is essential to deal with high food demand, for example, designing and utilizing agrochemicals that increase the nutrients in soils and improve crop growth by the eradication of crop-damaging organisms such as insects, fungi, pathogen bacteria, and undesirable weeds. However, the uncontrolled and excessive usage of these agrochemicals has led to serious environmental pollution, aquatic ecosystem degradation, and poisoning of some organisms.[2]

For instance, GLY is a broad spectrum herbicide and one of the most-used active weed killer substances.[3] Recently, awareness of its potential hazardous side effects such as endocrine disruption,[4] oxidative stress, DNA damage,[5] dermatological and respiratory issues,[6] and probably being carcinogenic to humans[7] have been a central discussion around the world, to such an extent that some countries have banned its use.[8] Thus, it is important to develop technologies and strategies for the efficient removal of GLY from ecosystems to protect human health and restore the affected habitats by this compound.

Wastes and residues are produced in our everyday activities, and it is vital to properly manage them to mitigate their environmental impact. In the meat industry, one of the most abundant byproducts is bones, which have historically been used

in animal feed and fertilizer production.[9] However, as it is a biological residue, some problems arise due to its inadequate biological stability, potential for rapid oxidation, high level of enzyme activity, and potentially pathogenic nature.[10] In fact, the food crisis that arose in Europe due the outbreak of bovine spongiform encephalopathy is a clear example of the pathogenic nature of this type of biological residues.[11] Therefore, other applications such as adsorbents' synthesis have been used as an alternative for bone waste management.[12−15]

Bone is a complex multifunctional connective tissue that plays several highly specialized functions in animal bodies. It is considered a natural organic−inorganic nanocomposite, the organic phase (25−37% wt) of which consists in collagen, glycoproteins, proteoglycans, sialoproteins, and bone "gla" proteins.[16] In contrast, the inorganic or biomineral phase (65−70% wt) is principally composed of calcium apatite nanocrystals very similar to the geologically occurring hydroxyapatite (Hap) but with some important chemical and structural differences.[17] These characteristics make bone waste a striking precursor for low-cost material obtention.
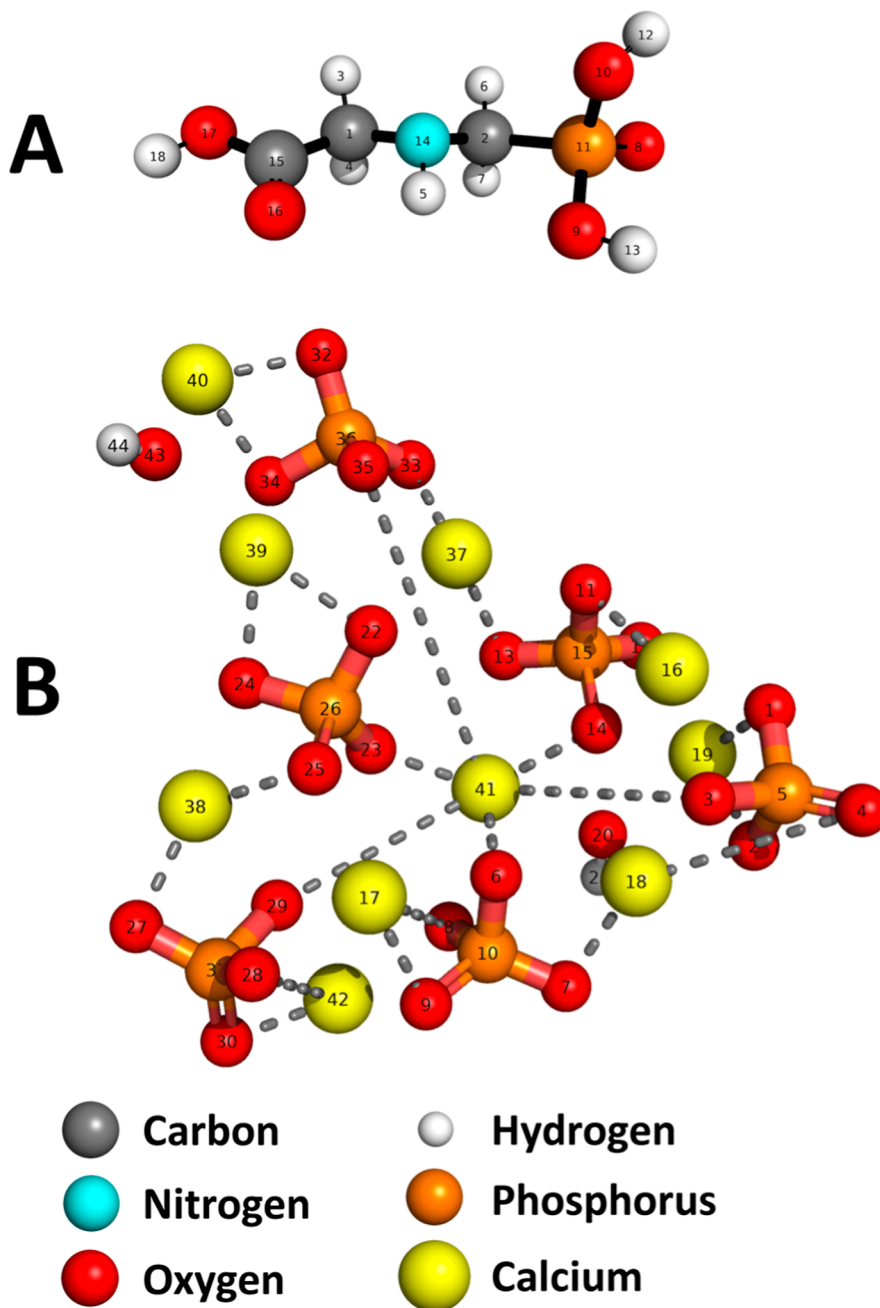
Biogenic hydroxyapatite (BHap) is a nanomaterial as it is found as nanocrystals embedded in collagen fibrils. It has received much attention because of its potential in biotechno-
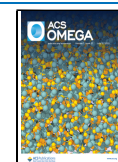
Figure 1. (A) Glyphosate and (B) hydroxyapatite optimized structures.

logical and biomedical applications. Thus, Hap surface interaction with some biomolecules and biochemicals, such as amino acids, has been studied by some researchers, finding high affinity between these kind of compounds and the Hap surface. Because of the similarity between GLY and amino acid molecular structures, it was of our interest to study the interaction between GLY and the BHap surface, obtained from cattle bone wastes via CO$_2$-assisted pyrolysis. The interaction was investigated by computational and experimental studies using density functional theory (DFT) calculations and immersion calorimetry, respectively.

2. THEORETICAL AND EXPERIMENTAL DETAILS

2.1. Density Functional Theory Calculations. To study the interaction between GLY and BHap, DFT, as implemented in the GAUSSIAN 09 package,[18] was used. The ground state of each system was obtained by calculating the total energy; to do that, the B3LYP[19] hybrid functional and 6-31g(d) basis set were employed. To model the interaction between GLY and BHap, the GLY molecule was set in different sites around the BHap structure, without any symmetry constraints. The total energy was calculated; that of the lowest energy was used to obtain the physicochemical properties. All the inputs were generated with GaussView 6.0. The absence of imaginary frequencies in the lowest total energy configuration was the criterion for ensuring stability. The structural parameters and the theoretical IR spectrum are also reported.

2.2. BHap Preparation. BHap was obtained from cattle bone waste, collected from a local butcher shop (Bogotá, Colombia), using the following methodology. First, bone wastes were subjected to hydrothermal treatment under controlled

pressure and temperature to remove the marrow, soft tissues, fats, and fluids. They were then dried at 100 °C for 48 h. Size reduction was done by crushing bone wastes with a hand-drilling hammer and subsequent milling using a blade mill of local construction. The obtained powders were washed several times with warm distilled water, dried at 100 °C for 48 h, and sieved. Finally, the raw bone powder (RBP) with a particle size between 1000 and 2000 μm was subjected to pyrolysis under a partially oxidative atmosphere (CO_2) using a tubular furnace Barnstead Thermolyne 21100 at a maximum temperature of 850 °C for 2 h, a heating rate of 5 °C·min^{-1}, and a CO_2 flow of 150 mL·min^{-1}.

2.3. Physicochemical Characterization. Thermogravimetric analysis was performed using a Hitachi STA 7200 thermal analysis system under a constant CO_2 flow of 150 mL min^{-1} and a heating rate of 5 °C·min^{-1} from 20 to 900 °C. Elemental analysis (C, H, N) was performed using a Thermo Scientific Flash 2000 elemental analyzer. Fourier transformed infrared (FT-IR) spectroscopy measurements were taken using a Shimadzu IRTracer-100 spectrometer equipped with a PKI Technologies attenuated total reflectance (ATR) accessory. Spectra were acquired between 400 and 4000 cm^{-1} with a resolution of 1.93 cm^{-1} and 100 scans to increase the spectra resolution. Raman spectroscopy measurements were taken with a Horiba Xplora Raman microscope using a 523 nm laser, 100× magnification, and 100% of laser power. X-ray powder diffraction (XRPD) was performed using a PANalytical X'Pert Pro MPD diffractometer with an X-ray source of Cu (λ = 1.5406 Å). Diffractograms were acquired in the 2θ range of 5−90° with a step size of 0.02°. Scanning electron microscopy (SEM) images were obtained using a TESCAN LYRA3 FIB-SEM microscope, equipped with a microanalysis system of energy-dispersive X-ray spectroscopy (EDS).

Determination of the point of zero charge (pH_{PZC}) was done following the salt addition method with slight modifications.[20] First, a stock solution of NaCl 0.01 M was prepared. The initial pH_0 was adjusted to values between 2 and 11 by the addition of some droplets of HCl o NaOH 0.10 M solutions. N_2 gas was bubbled into each solution to remove the dissolved CO_2 and avoid interferences in the pH measurements. Then, 25 mg of BHap was added to 15 mL of each solution with different pH_0. After 72 h of constant shaking, solutions were filtered and final pH_f was measured. pH_{PZC} was determined by plotting the difference between pH_f and pH_0 (ΔpH) against pH_0. The pH in which ΔpH equals zero corresponds to pH_{PZC}. These measurements were performed using a Hanna Instruments HI 2211 pH-meter; the electrode was calibrated using standard buffer solutions of pH 4, 7, and 10.

The nitrogen physisorption isotherm at −196 °C was measured using a gas sorption analyzer Quantachrome Autosorb IQ2. Before analysis, 100 mg of BHap was outgassed under vacuum (10^{-5} mbar) using two heating steps: the first one up to 100 °C with a heating rate of 2 °C·min^{-1} (evacuation phase) and the second one from 80 to 200 °C with a heating rate of 5 °C·min^{-1}, holding this temperature for 9 h (heating phase). Then, sorption analysis was carried out acquiring a 51-point isotherm, 30 of the adsorption branch, and 21 of the desorption branch. Specific surface area was determined applying the Brunauer−Emmett−Teller (BET) equation in the 0.05−0.3 range of relative pressure.

Immersion calorimetry was performed using a Calvet-type microcalorimeter of local construction.[21] A sample of 200 mg of BHap was introduced in a glass ampule with a filament at the end. Then, the stainless steel cell was filled with 10 mL of the immersion liquid, and the ampule was placed inside. The lid was set on the top of the calorimeter, and the electrical potential was measured every 2 s until the baseline was constant and uniform. Afterward, an ampule filament was broken with the bottom of the cell to immerse the solid into the liquid (solution) and measure the electric potential change that results of the solid−liquid interaction (thermal effect). After immersion, calibration was done by supplying an electrical power to the system [known potential (V), current intensity (I), and time (t)] and measuring the electric potential change to determine the calorimeter constant K_{cal} (eq 1). Immersion enthalpies were calculated using the area under the peak (immersion energy) in each potentiogram as follows (eqs 1−3)

$$K_{cal} = \frac{\text{calibration energy}}{\text{calibration peak area}} = \frac{V \times I \times t}{\text{calibration peak area}} \quad (1)$$

$$E_{imm} = K_{cal} \times \text{immersion peak area} \quad (2)$$

$$\Delta H_{imm} = \frac{E_{imm}}{\text{solid's mass}} \quad (3)$$

Immersion liquids were water, HCl at different concentrations, and solutions of GLY analytic reagent and commercial formulation. Each measurement was carried out in triplicate.

3. RESULTS AND DISCUSSION

3.1. Computational Simulation Results. *3.1.1. Structural Properties.* Figure 1 shows the optimized molecular structure of GLY and Hap; the initial structure for GLY was taken from Knuuttila et al.'s work[22] and for Hap from Ozturk et al.'s work.[23] In all cases, no imaginary frequencies were found, which confirm the system stability. Neutral charge (q = 0) and multiplicity (singlet) yielded the molecules to the ground state. Further studies were developed with these molecular structures.

The molecular structure of glyphosate (GLY) has the typical zig−zag form; Table S1 contains their ground-state intramolecular distances and angles, which is in good agreement with experimental and theoretical values.[22,24] The P−C bond has the value 1.822 Å, while the reported experimental and theoretical values are 1.823 and 1.827 Å, respectively. The C−H bonds range from 1.096 to 1.109 Å, while the N−H bond has the value 1.017 Å. Small deviations from experimental values were found in the phosphonic group. The obtained P11−O9 and P11−O10 bond lengths have very similar values (1.627 Å), which indicates a resonance between the two O atoms;[22] the experimental value is 1.500 Å. A larger discrepancy was found in the P11=O8 bond, with 1.627 Å being our result and 1.576 Å being the experiment value; some divergences between our results (0.972 Å) and the experimental value (0.711 Å) were also noted in the O−H bonds. This result may be due to the fact that the calculations were done in the isolated form of GLY,[22] and the interaction with neighboring molecules was neglected. Additionally, our calculated angle bonds also coincide with the reported values; as an example, the theoretical O−P−O angles range from 102.485 to 118° and the experimental values are in the range 106.0−118°.

Six phosphate groups, whose P−O bonds are in the range 1.53−1.63 Å, compose Hap; other DFT calculations obtained with this parameter are in the range 1.54−1.66 Å.[23] Our calculated Ca−O bonds (2.32−2.52 Å) and O−Ca bonds (2.28−2.50 Å) as well as O−H (0.97 Å) are also in good accordance with the reported values (presented in Table S2). The angles of the O−P−O bonds are reported in the range
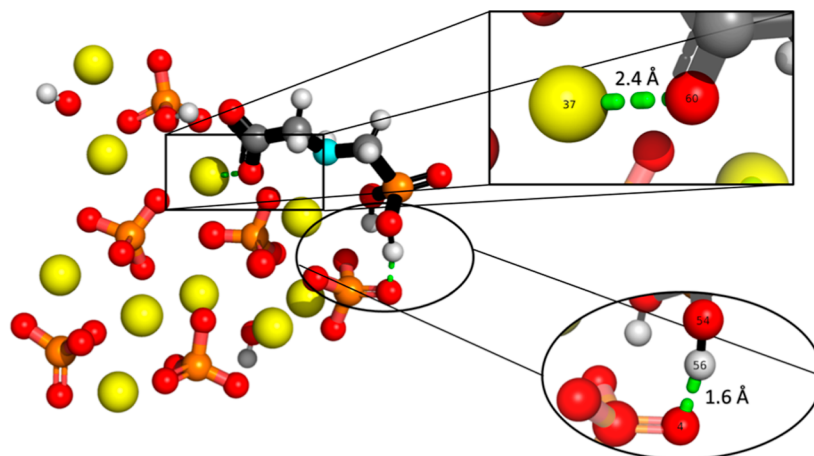
Figure 2. Lowest energy configuration of the interaction of Hap−GLY.

102.05−113.26°, while our calculated values are in the range 102−120.2°; similar agreement was found in the O−Ca−O angle bonds (75.06−143.55° in the literature and 54.23−143.01° in our calculations).

3.1.2. Hydroxyapatite Interaction with GLY. The interaction between these two systems was studied placing the optimized structure of GLY on the optimized structure of Hap; this approach has been widely used to model the interaction of GLY with many other systems with successful results.[25−27] The complex was analyzed using the B3LYP functional with the 6-31g(d) basis set. The as-obtained system was optimized to the lowest energy structure (Figure 2). The adsorption energy (E_{ads}) of GLY on Hap, obtained with eq 4, has the value −2.672 eV, which is associated with exothermic chemisorption.

$$E_{ads} = E_{Hap-GLY} - E_{GLY} - E_{Hap} \tag{4}$$

where E_{ads} is the energy of adsorption, $E_{Hap-GLY}$ is the total energy of the Hap−GLY system, E_{Hap} is the Hap total energy, and E_{GLY} is the GLY total energy.

The Hap−GLY interaction is developed between the Ca37 (Hap) atom and O60 of the carboxyl group (GLY), whose distance is 2.45 Å; this is the average value for the Ca−O bond in Hap. In the isolated form of Hap and GLY, Ca37 has the charge 1.12 e and O60 0.45 e; in the interaction, the charges of Ca and O atoms change to 1.07 and −0.66 e, respectively. This fact generated the attraction of GLY to Hap. Also, one hydrogen atom (H18) transferred from the carboxyl group to the phosphate group (H62). Besides this phenomenon, the absence of structural changes in Hap as well as in GLY after the interaction was noted.

The interaction between Hap and GLY was also analyzed by the infrared (IR) spectrum. Normal modes of individual molecules as well as the coupled system after optimization are shown in Figure 3. Our results of Hap and GLY are very close to data reported in the literature.[23,26] The main normal modes found in the range 500−1500 cm^{-1} of the Hap−GLY system are consistent with that found for the isolated Hap and GLY. The H atom that transferred from GLY to Hap formed an O−H stretching bond, characterized by the signal at 3202 cm^{-1}. The interaction between Ca37 (Hap) and the atom O60 of the carboxyl group (GLY) is related to the 1704 and 1417 cm^{-1} vibrational modes. This result confirmed the existence of coupled vibrations in the Hap−GLY system, as predicted in the adsorption energy calculations. Finally, intense peaks at 2528
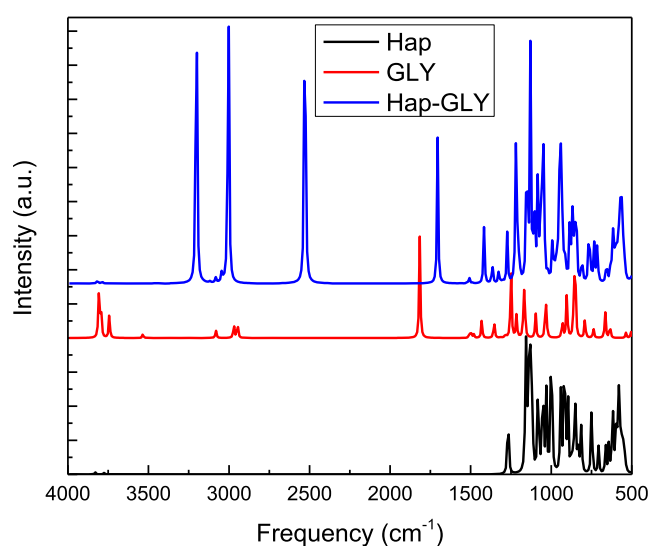
Figure 3. Infrared intensities calculated of Hap and GLY isolated and the Hap−GLY system.

and 3003 cm^{-1} correspond to the O−H stretching bonds in the phosphonic group.

3.2. Experimental Results. *3.2.1. Physicochemical Characterization.* Figure 4 shows the ThermoGravimetric (TG) and Differential ThermoGravimetry (DTG) plots for RBP under a CO_2 atmosphere. It is possible to note three distinctive weight loss zones. Zone I (20−200 °C) is attributed to loss of adsorbed volatile molecules and moisture, with a maximum mass loss of 6.2% and a maximum mass loss rate of −0.04%/°C reached at 92.5 °C. Thermal degradation of the organic structure composed of substances such as molecular chains of collagen, proteins, and fat tissue is presented between 200 and 576 °C (Zone II). In this region, the highest mass loss percentage (22.4%) is found, with also the highest mass loss rate at 331 °C. Finally, Zone III goes from 576 to 880 °C. The weight loss in this zone is owing to the partial dehydroxylation process of Hap and the decomposition of carbonates.[28] The mass loss in this temperature range is about 6.6% and the maximum rate of mass loss is located at 781 °C.

These results show the thermal behavior of RBP under a CO_2 atmosphere and are useful for the proper selection of the pyrolysis conditions to obtain BHap. As mentioned previously, in the third zone, the mass loss is due to the decomposition of
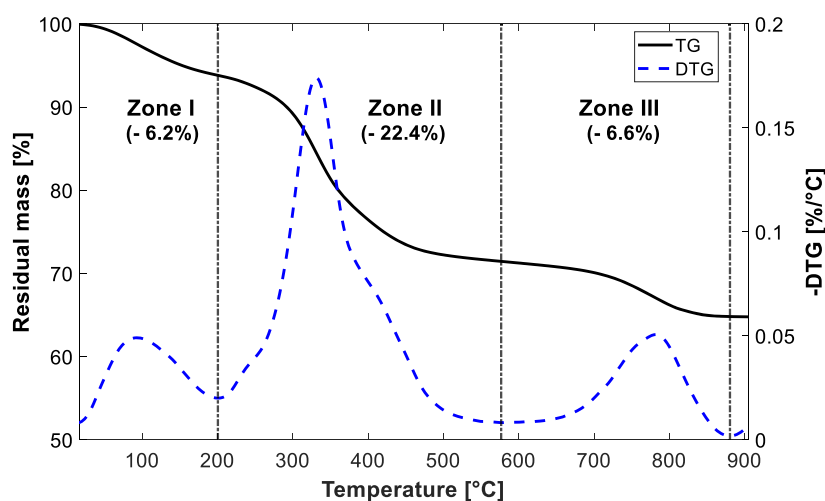
Figure 4. TGA-DTG of RBP under a CO_2 atmosphere.

carbonates and partial dehydroxylation of Hap. It is worthwhile to mention that to obtain BHap with a structure and chemical composition similar to that of geological Hap, it is necessary to guarantee the complete elimination of the organic content from the RBP as well as the decomposition of carbonates. According to the analysis, 850 °C is an optimal pyrolysis temperature to obtain BHap under a partially oxidative atmosphere (CO_2).

Pyrolysis yield was around 60−62%, which is in accordance with the final mass percentage calculated with the TGA. Samples of RPB are yellow-pale, and after thermal treatment, the typical white color of Hap is obtained, as observed in Figure 5. This color change is associated with the degradation of the organic matrix, leaving BHap as the product.

Figure 5. Photographs of (A) RBP and (B) BHap (photographs taken by the authors).

Elemental analysis of RBP shows that it has carbon, nitrogen, and hydrogen contents of 16.61, 6.90, and 2.75% wt, respectively, while in BHap, these percentages are reduced to 0.51, 0.39, and 0.01% wt, respectively. The decrease of these percentages is owing to the thermal decomposition of proteins presented in the RBP structure as well as the degradation of carbonates during thermal treatment under a CO_2 atmosphere, showing that the resulting BHap corresponds to the inorganic matrix of RBP.

The FT-IR spectra are shown in Figure 6, where several differences are identified. The RBP spectrum shows a broad band between 3600 and 3000 cm^{-1}, characteristic of the hydroxyl (−OH) functional group; bands between 1700 and 1400 cm^{-1} correspond to C═O, C═C, and C═N vibrations, all of them associated to collagen and other proteins. The inorganic phase of RBP is evidenced in the strong band between
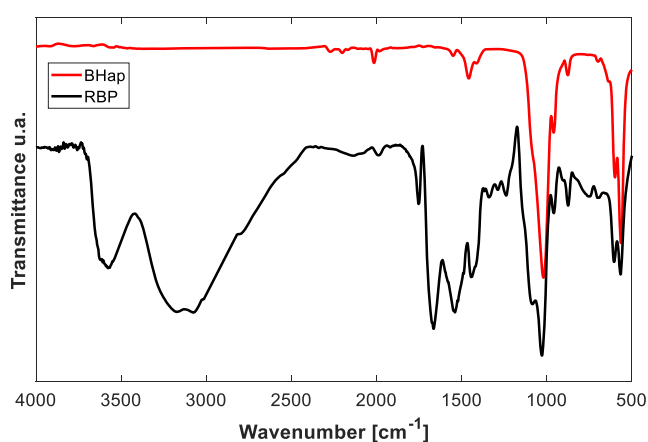

Figure 6. FT-IR spectra of RBP and BHap.

1150 and 900 cm^{-1} that corresponds to phosphate (PO_4^{3-}) vibrational modes, the band at 565 cm^{-1} corresponds to calcium and phosphate bonds, and the bands at 1300−1200 and 720 cm^{-1} are due to the presence of carbonate (CO_3^{2-}).[29] The bands associated with the inorganic phase are also found in the BHap spectrum, with insignificant differences, confirming that Hap was generated successfully with the CO_2-assisted pyrolysis. Some authors attribute the shoulder located at 1100 cm^{-1} to the degree of crystallinity of the Hap;[30] because of the absence of this shoulder in the BHap spectrum, there is an increase in the crystallinity of BHap after thermal treatment. The clear nonappearance of the bands associated with C═O, C═C, and C═N bonds (between 1700 and 1400 cm^{-1}) in BHap confirms the thermal degradation of the organic matrix. The dehydroxylation is confirmed by the lack of the −OH band, while the reduction in the intensities of the CO_3^{2-} bands indicates the thermal degradation of carbonates.

The Raman spectra of RBP and BHap are shown in Figure 7. The intense characteristic band at 960 cm^{-1} corresponds to the stretching ν_1 of the phosphate group, and as can be seen, there is an increase in the intensity of this band in the BHap spectrum. This result demonstrates that the crystallinity indeed increases as proposed previously with FT-IR. On the other hand, the band located at 590 cm^{-1} is attributed to the ν_4 stretching of the phosphate tetrahedra. The weak band located at 1070 cm^{-1} is
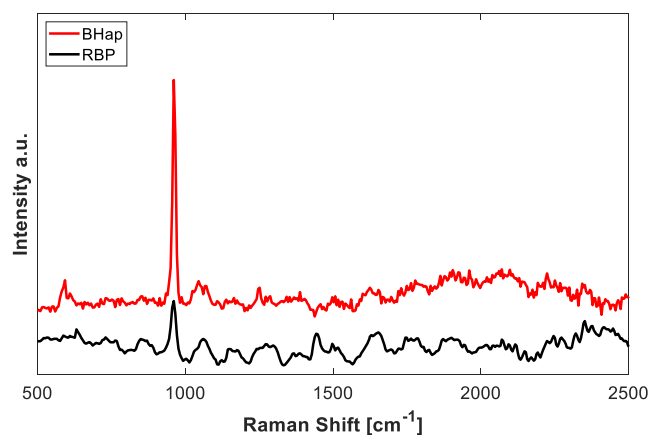
Figure 7. Raman spectra of RBP and BHap.

assigned to the CO_3^{2-} presence, which agrees with the band of the FT-IR spectra and with the literature.[31]

The BHap diffractogram is shown in Figure 8 together with the reported Hap diffraction patter (Crystallographic Open
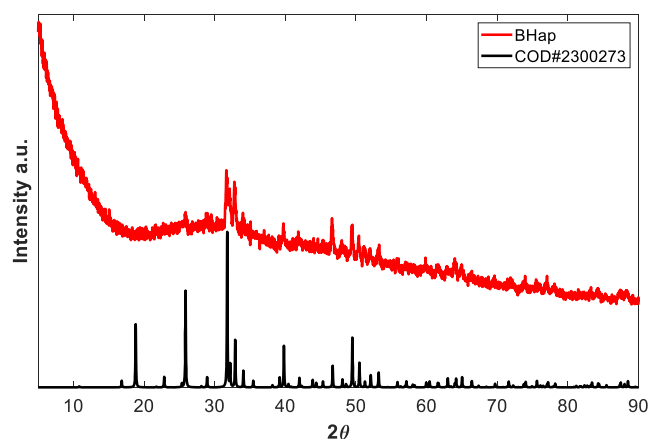

Figure 8. X-ray diffraction pattern of BHap and Hap (COD#2300273).

Database COD#2300273). From the XRDPD patterns, it is possible to prove the presence of Hap in the BHap sample, presenting a characteristic hexagonal Bravais lattice with space group $P6_3/m$. The most intense diffraction peaks in the diffractogram are at two values of 25.8, 28.9, 31.7, 32.1, 32.9, 34.0, 39.8, 46.7, 49.4, and 50.5°, which are described by the following Miller indices (002), (021), (211), (300), (202), (310), (222), (312), and (213), respectively. It is worth noting that there is no peak shifting, indicating that the unit cell had neither shrunk nor expanded compared to Hap. The difference in the peaks' relative intensities indicates a variation in the BHap's atomic structure, probably by vacancies of some groups such as Ca^{2+}, PO_4^{3-}, and OH.
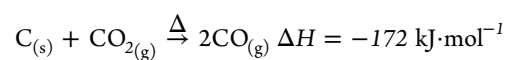
SEM micrographs of BHap are shown in Figure 9. The BHap surface is characterized by roughness and heterogeneity (Figure 9A); some cavities and fractures on its surface are also observed (Figure 9B,D). In some regions, disorganized laminar-shaped structures are found (Figure 9B), which come from the original bone matrix (RBP). A magnification of 40,000× (Figure 9C) permits one to observe in detail the micro−nano structure of BHap. As seen there, it is composed of nanosized particles of Hap that are attached to each other due to the coalescence process that takes place at the pyrolysis temperature used (850

°C).[32] It is possible to observe the grain boundaries between each nanoparticle and some voids or cavities formed between them. In Figure 9D,E a different BHap particle is observed, in general, with the same characteristics as the other one, indicating homogeneity in the sample. A special feature is highlighted in Figure 9E, revealing the presence of collagen fiber-like structures that remain after thermal treatment, clearly without organic composition, thus composed of BHap.

The EDS analysis confirms the chemical composition of the obtained material. The elemental mapping (Figure 10) shows that even though BHap has a heterogeneous and rough surface, its chemical composition is homogeneous, as it is observed that all the atoms are distributed uniformly over the surface. The EDS spectrum shows that O, Ca, P, C, and traces of Mg and Na are present in BHap, in a mass percentage of 41.69, 37.21, 16.45, 3.23, 0.85, and 0.57% wt, respectively. Mg and Na are natural ions commonly found in a bond matrix, and so they are present in BHap. The Ca/P ratio is a very important parameter commonly determined when Hap is synthesized because it is directly related to the stoichiometry of Hap. According to its molecular formula, the Ca/P atomic ratio must be 1.67. In this case, Ca and P have atomic percentages of 21.15 and 12.07%, respectively, which gives a Ca/P ratio of 1.75. This value shows that BHap is not stoichiometrically identical to Hap, probably to a smaller content of phosphate groups or a higher content of calcium, which explains some of the differences observed in XRPD patterns. Similar results have been reported for Hap obtained from other natural resources (i.e., fish scales, eggshells, sea shells, etc.).[33]

Nitrogen physisorption isotherm at −196 °C of BHap is shown in Figure 11. According to the IUPAC technical report,[34] it is classified as a Type III isotherm, characteristic of systems with no porosity or macroporosity, with a weak interaction between N_2 and the BHap surface. The BET specific surface area was determined to be 5 $m^2 \cdot g^{-1}$, which is consistent with the low surface areas reported for this type of materials.[35,36] Finally, it was determined that BHap presents a basic nature because of its high pH_{PZC} of 9.7. The basicity of this material is due to the presence of groups such as phosphates (PO_4^{3-}) and carbonates (CO_3^{2-}). pH_{PZC} is a very important property in surface processes because it describes the behavior of the surface charge according to the solution pH. When pH > pH_{PZC}, the surface is negatively charged, and conversely, when pH < pH_{PZC}, the surface has a positive charge.

With the results presented so far, it may be concluded that the pyrolysis of bone waste assisted with CO_2 is an appropriate technique to obtain this type of material. An advantage of using CO_2 as the pyrolysis atmosphere gas is that the organic matrix is totally degraded due to the gasification reactions promoted by CO_2 at 850 °C. In contrast, pyrolysis under an inert atmosphere (N_2) and under the same experimental conditions gives as the product a dark material, known as bone char, whose carbon content is in the range of 10−12%.[37] The gasification reaction that takes place in CO_2 pyrolysis is known as the Boudouard reaction, described in the following reaction

$$C_{(s)} + CO_{2(g)} \xrightarrow{\Delta} 2CO_{(g)} \ \Delta H = -172 \text{ kJ} \cdot \text{mol}^{-1}$$

The thermal degradation of carbonates is expected to happen at temperatures higher than 700 °C, and it is described by the following reaction
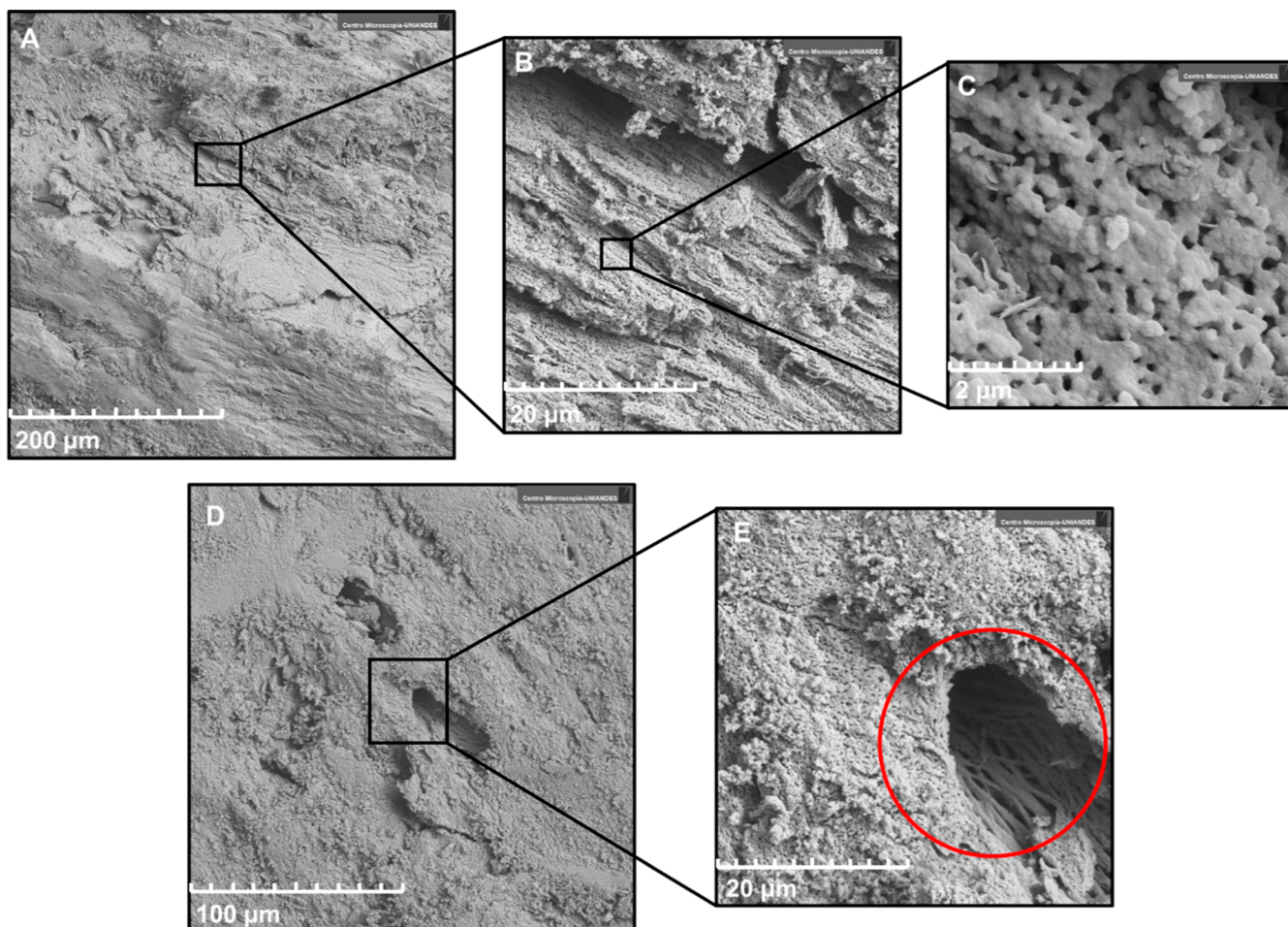
Figure 9. SEM micrographs of BHap with a backscattering electron detector and 10 kV. (A) Magnification of 500× (particle I), (B) magnification of 5000× (particle I), (C) magnification of 40,000× (particle I), (D) magnification of 1000× (particle II), and (E) magnification of 5000× (particle II).
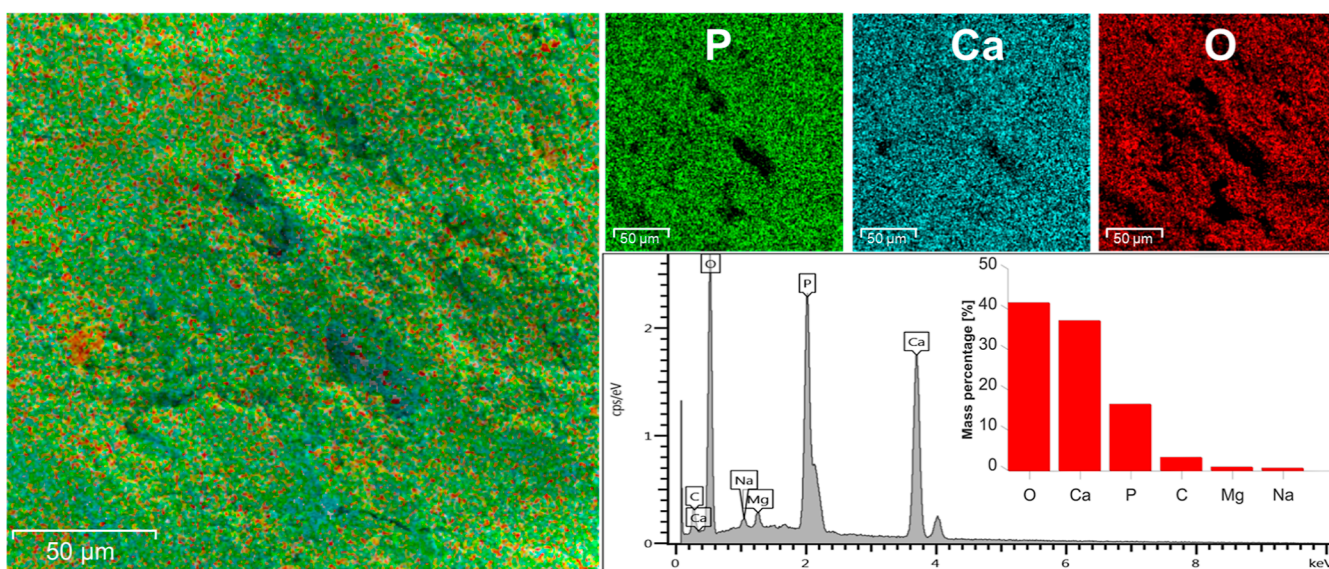
Figure 10. EDS mapping, EDS spectra, and element composition percentage.

$$CaCO_{3(s)} \xrightarrow{\Delta} CaO_{(s)} + CO_{2(g)}$$
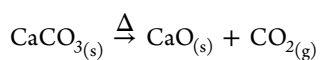
However, according to Le Chatelier's principle, this reaction is not favored as pyrolysis is under a CO_2 atmosphere. This is an advantage of this methodology in comparison to thermal treatment under oxidative atmosphere (calcination) because it avoids the formation of calcium oxide and, in general, other oxides such as magnesium oxide. In addition, as determined via
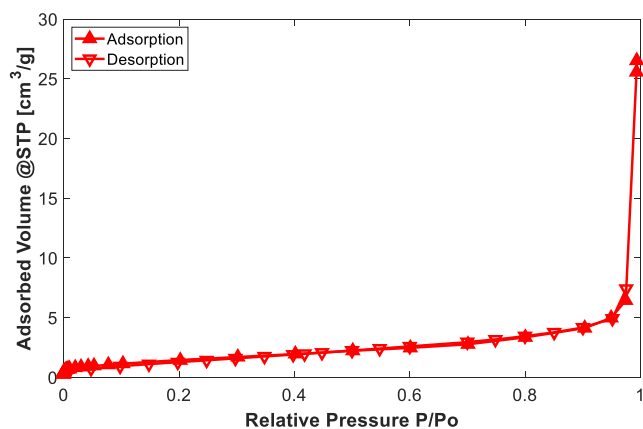
Figure 11. Nitrogen adsorption−desorption isotherm at −196 °C.

Figure 12. Potentiograms obtained from immersion of BHap in HCl solutions of different concentrations.

FT-IR, in this case, partial degradation of carbonates happens under the pyrolysis conditions used.[38]

3.2.2. Immersion Calorimetry: Interaction of GLY and BHap. The interaction between GLY and BHap was investigated by means of immersion enthalpies, as a way of looking for potential adsorbents of GLY from water. Immersion calorimetry consists of measuring the heat transferred when a solid is immersed in a liquid, such as water, organic solvents, or any aqueous solution. The thermal effect is measured and correlated to the immersion enthalpy, which is a thermodynamic parameter that depends on the system under study. Principally, it depends on the textural properties and surface chemistry of the solid as well as on the nature of the immersion liquid.[39]

In general, immersion enthalpy is proportional to the surface area of the solid, which in our case is a very low surface area (5 $m^2 \cdot g^{-1}$). This was a limiting factor in our experiments, so we had to increase 4 times the mass of BHap in each experiment. However, in the case of immersion in water, no thermal effect was observed, indicating a weak interaction between water molecules and the BHap surface. It is well known that bone Hap must have a hydrophilic nature owing to the cell proliferation that must be guaranteed as it is a biological tissue.[40] In calorimetric studies of different samples of Hap immersed in water and n-decane, the hydrophilic character of the Hap was demonstrated.[41] This discrepancy is explained by the difference in the surface chemistry, structure, and morphology between the BHap obtained from bone waste and the synthetic Hap obtained from the hydrothermal reaction of calcium acetate and potassium hydrogen phosphate. Specifically, the surface area of the Hap obtained by Skwarek et al.[41] is almost 6 times higher than BHap's surface area, expounding the lower or absence of thermal effect of the immersion of BHap in water.

The same behavior was observed when BHap was immersed in other solvents such as benzene, ethanol, and NaOH 0.1 M solution, which is also related to the low surface area, hydrophilicity, and basicity. By contrast, a thermal effect was observed when BHap was immersed in acidic solutions of HCl, as shown in Figure 12.

The thermal effect measured with the immersion of BHap in HCl solutions is not only due to the neutralization of surface basic groups but also the dissolution of BHap. Calcium apatites are not stable in acidic medium, and this process is influenced by factors such as the pH, concentration, saturation, chemical composition, solubility, particle size, surface defects, and the crystal phase, among others. Eight models have been reported in the literature, namely, diffusion and kinetically controlled,
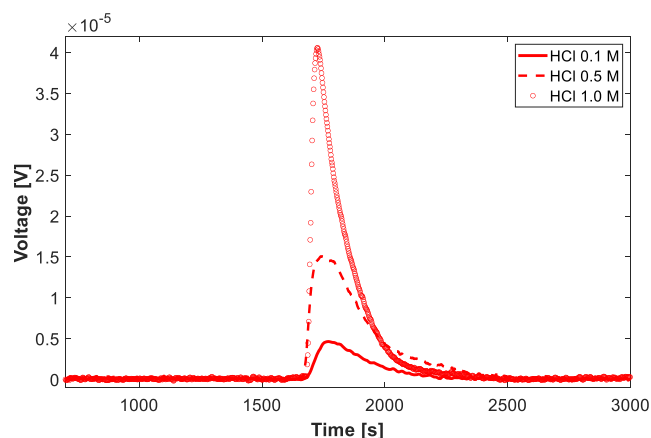
mono- and polynuclear, stoichiometric/non-stoichiometric dissolution, chemical model, self-inhibition, etch pit formation, ion exchange model, and hydrogen catalytic model. All of them have advantages and drawbacks, and their validity depends on the different assumptions and specific conditions in which they are based.[42] Recently, a generalized dissolution mechanism was proposed, in which the previous models were summarized and combined to explain completely the acid dissolution process.[42] Concisely, after Hap is placed into an acidic aqueous solution, sorption of water molecules and ions (H^+ and Cl^-) takes place; then, a chemical transformation occurs on the Hap surface, the detachment of lattice ions from a kink site, and finally diffusional steps away from the crystal toward the bulk solution.

The thermodynamics of acid dissolution have been studied by some authors, specially related to the kinetics and rate of dissolution of Hap.[43−45] In addition, an investigation about the enthalpies of solubilization of Hap was made by Ardhaoui et al.[46] They found that there is a proportional relation between the acid concentration and the measured enthalpy. It is worth noting that conditions used there differ from the conditions used in the present work. We observed no total dissolution of BHap due to the high amount of solid that was required to detect the thermal effect in a cell of 10 mL, and for that reason, results are not totally comparable. However, the same trend was obtained with an enthalpy of immersion ($-\Delta H_{imm}$) of 6.6 ± 0.9, 29.6 ± 1.7, and 41.4 ± 1.5 $J \cdot g^{-1}$ for the HCl solution of 0.1, 0.5, and 1.0 M, respectively. The tendency is caused by the less quantity of basic groups of BHap required to neutralize the H^+ ions, while a higher concentration of HCl reacts with a higher quantity of basic groups, solubilizing more BHap.

On the other hand, immersions in 20 mM solutions of GLY were carried out, and the corresponding potentiogram is shown in Figure 13. Interestingly, a thermal effect was found unlike the immersion experiment in water, despite them being aqueous solutions. This means that there is an interaction between GLY and the BHap surface, strong enough to be measured and clearly stronger than that of water molecules and BHap. From the potentiogram (Figure 13), the calculated $-\Delta H_{imm}$ for each solution has average values of 8.3 ± 0.8 and 4.1 ± 1.1 $J \cdot g^{-1}$ for the solutions of commercial GLY and the analytical reagent, respectively. The $-\Delta H_{imm}$ of commercial GLY solution is almost twice the enthalpic value of the analytical reagent system; this difference is associated with the composition of the commercial formulation, which contains other substances
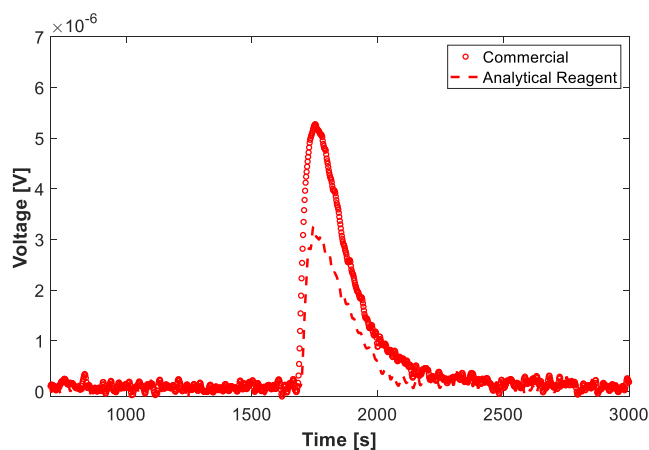
Figure 13. Potentiogram obtained from the immersion of commercial GLY and the analytical GLY reagent (20 mM).

besides GLY, named as "inert" components. These substances are in greater proportion surfactants that promote the uptake of the herbicide by plants cells, such as polyoxyethylene tallow-amine and metals such as As, Co, Cr, Ni, and Pb.[47] This co-formulant can interact with BHap during the immersion, resulting in a more exothermic process compared to analytical GLY solutions.

With the obtained results so far, it may be concluded that BHap has potential applications in some areas like adsorption for water depuration, specifically in the adsorption of GLY. Another important feature is that the interaction with BHap and GLY is stronger than the interaction of this material with water, which is favorable in adsorption processes in the aqueous phase, because it is necessary to exchange the surface adsorbed water molecules with the adsorbate molecules (GLY) for adsorption to take place.

Other Haps have been obtained using different methodologies. For example, Hap obtained by the reaction of eggshell powder ($CaCO_3$) with HNO_3 at 800 °C, in conjunction with aqueous ammonia and H_3PO_4, is also effective for adsorbing GLY.[48] This Hap presented a BET specific surface area of almost 100 times higher ($566 \ m^2{\cdot}g^{-1}$) than the one obtained in the present work. With this Hap, the authors obtained a promising GLY adsorption capacity of $890 \ mg{\cdot}g^{-1}$.

Owing to the biological applications of Hap, its adsorption capacity has been studied using compounds such as amino acids, which motivated the present work due to their molecular structure similarity with GLY. In fact, GLY's IUPAC name is *N*-(phosphonomethyl) glycine, being a derivative of the amino acid glycine. As an example, adsorption of glycine and glutamic acid was studied by means of molecular dynamics.[49] In that work, they found that at an atomistic level, amino acids are adsorbed over specific crystals facets of Hap, with their positive-charged amino groups on calcium vacant sites, while negatively charged carboxylate groups occupy phosphate vacancies. In addition, adsorption of L-lysine and DL-leucine was studied onto a poorly crystallin Hap obtained using the precipitation method.[50] The main conclusions were that the charged carboxylate and amino moieties are the groups responsible in the interaction with the Hap surface, being governed by electrostatic interactions. Finally, binding free energies and binding mechanisms of 20 natural amino acids were studied using dynamic simulations,[51] concluding that charged amino acids bind stronger than neutral amino acids. Also, it was confirmed that the affinity of this kind of molecules with the Hap surface depends directly on its ability to replace adsorbed water molecules.

4. CONCLUSIONS

BHap obtained from cattle bone waste was successfully obtained via CO_2-assisted pyrolysis, and it was fully characterized as a calcium apatite very similar to Hap. We conclude that this is a promising material for the adsorption of GLY in aqueous solutions. It was demonstrated experimentally that there is an interaction between GLY molecules and BHap and that, indeed, it is stronger than the interaction with water molecules, which is vital for adsorption to take place. Complementarily, a computational study was carried out with the purpose of studying the interaction between BHap and GLY, finding that there is strong adsorption (chemisorption) between these compounds, which proves the high affinity of GLY and the BHap surface.

Here, we showed that BHap is a promising adsorbent for remediation of water polluted with GLY. The positive environmental impact of this work is evident in the fact that we propose the depuration of water sources by adsorption, utilizing and valorizing animal bone wastes as adsorbents. In this way, two different problems are faced at the same time: polluted water treatment and solid waste management.

For further works, it is necessary to study the adsorption of GLY into Hap by the experimental determination of the adsorption isotherms in the aqueous phase. In addition, as reviewed in literature, surface area is a critical parameter during adsorption, so modifications of BHap must be performed to increase the surface area, without losing the surface functional groups of BHap.

■ ASSOCIATED CONTENT

ⓢ Supporting Information
The Supporting Information is available free of charge at https://pubs.acs.org/doi/10.1021/acsomega.2c01379.

    Structural parameters obtained for GLY and hydroxyapatite by DFT calculations (PDF)

■ AUTHOR INFORMATION

Corresponding Author

Juan Carlos Moreno-Piraján − *Departamento de Química—Facultad de Ciencias, Universidad de Los Andes, Bogotá 11711, Colombia;* ⓞ orcid.org/0000-0001-9880-4696; Phone: (571) 3394949 Ext. 3465; Email: jumoreno@uniandes.edu.co

Authors

Diego F. Hernández-Barreto − *Departamento de Química—Facultad de Ciencias, Universidad de Los Andes, Bogotá 11711, Colombia*

Heriberto Hernández-Cocoletzi − *Facultad de Ingeniería Química, Benemérita Universidad Autónoma de Puebla, Puebla 72570, Mexico*

Complete contact information is available at:
https://pubs.acs.org/10.1021/acsomega.2c01379

Author Contributions
J.C.M.-P and D.F.H.-B. conceived and design the experiments. H.H.-C. conceived, designed, and performed the computational simulations. D.F.H.-B. performed the experiments. J.C.M.-P., H.H.-C., and D.F.H.-B. analyzed and interpreted the results. The manuscript was written through contributions of all authors. All

■ ABBREVIATIONS

GLY   glyphosate
BHap   biogenic hydroxyapatite
Hap   hydroxyapatite
BET   Brunauer−Emmett−Teller
DFT   density functional theory

■ REFERENCES

(1) Bhat, R. Sustainability Challenges in the Valorization of Agri-Food Wastes and by-Products. *Valorization of Agri-Food Wastes and By-Products*; Academic Press, 2021; pp 1−27.

(2) Yu, T.; Ma, H.; Zhang, H.; Xiong, M.; Liu, Y.; Li, F. Fabrication and Characterization of Purified Esterase-Embedded Zeolitic Imidazolate Frameworks for the Removal and Remediation of Herbicide Pollution from Soil. *J. Environ. Manage.* **2021**, *288*, 112450.

(3) Carles, L.; Gardon, H.; Joseph, L.; Sanchís, J.; Farré, M.; Artigas, J. Meta-Analysis of Glyphosate Contamination in Surface Waters and Dissipation by Biofilms. *Environ. Int.* **2019**, *124*, 284−293.

(4) Ingaramo, P.; Alarcón, R.; Muñoz-de-Toro, M.; Luque, E. H. Are Glyphosate and Glyphosate-Based Herbicides Endocrine Disruptors That Alter Female Fertility? *Mol. Cell. Endocrinol.* **2020**, *518*, 110934.

(5) Mesnage, R.; Brandsma, I.; Moelijker, N.; Zhang, G.; Antoniou, M. N. Genotoxicity Evaluation of 2,4-D, Dicamba and Glyphosate Alone or in Combination with Cell Reporter Assays for DNA Damage, Oxidative Stress and Unfolded Protein Response. *Food Chem. Toxicol.* **2021**, *157*, 112601.

(6) Camacho, A.; Mejía, D. The Health Consequences of Aerial Spraying Illicit Crops: The Case of Colombia. *J. Health Econ.* **2017**, *54*, 147−160.

(7) IARC Working Group on the Evaluation of Carcinogenic Risks to Humans. *Some Organophosphates Insecticides and Herbicides*; International Agency for Research on Cancer, 2015; Vol. *112*, pp 1−464.

(8) Meftaul, I. M.; Venkateswarlu, K.; Dharmarajan, R.; Annamalai, P.; Asaduzzaman, M.; Parven, A.; Megharaj, M. Controversies over Human Health and Ecological Impacts of Glyphosate: Is It to Be Banned in Modern Agriculture? *Environ. Pollut.* **2020**, *263*, 114372 Elsevier Ltd August 1.

(9) Bujak, J. W. New insights into waste management - Meat industry. *Renewable Energy* **2015**, *83*, 1174−1186.

(10) Jayathilakan, K.; Sultana, K.; Radhakrishna, K.; Bawa, A. S. Utilization of Byproducts and Waste Materials from Meat, Poultry and Fish Processing Industries: A Review. *J. Food Sci. Technol.* **2012**, *49*, 278−293.

(11) Vamvuka, D.; Dermitzakis, S.; Pentari, D.; Sfakiotakis, S. Valorization of Meat and Bone Meal through Pyrolysis for Soil Amendment or Lead Adsorption from Wastewaters. *Food Bioprod. Process.* **2018**, *109*, 148−157.

(12) Sellaoui, L.; Dhaouadi, F.; Reynel-Avila, H. E.; Mendoza-Castillo, D. I.; Bonilla-Petriciolet, A.; Trejo-Valencia, R.; Taamalli, S.; Louis, F.; El Bakali, A.; Chen, Z. Physicochemical Assessment of Anionic Dye Adsorption on Bone Char Using a Multilayer Statistical Physics Model. *Environ. Sci. Pollut. Res.* **2021**, *28*, 67248.

(13) Maeda, C. H.; Araki, C. A.; Moretti, A. L.; de Barros, M. A. S. D.; Arroyo, P. A. Adsorption and Desorption Cycles of Reactive Blue BF-5G Dye in a Bone Char Fixed-Bed Column. *Environ. Sci. Pollut. Res.* **2019**, *26*, 28500−28509.

(14) Côrtes, L. N.; Druzian, S. P.; Streit, A. F. M.; Sant'anna Cadaval Junior, T. R.; Collazzo, G. C.; Dotto, G. L. Preparation of Carbonaceous Materials from Pyrolysis of Chicken Bones and Its Application for Fuchsine Adsorption. *Environ. Sci. Pollut. Res.* **2019**, *26*, 28574−28583.

(15) Thompson, M. O.; Kearns, J. P. Modeling and Experimental Approaches for Determining Fluoride Diffusion Kinetics in Bone Char Sorbent and Prediction of Packed-Bed Groundwater Defluoridator Performance. *Water Res.: X* **2021**, *12*, 100108.

(16) Sommerfeldt, D.; Rubin, C. Biology of Bone and How It Orchestrates the Form and Function of the Skeleton. *Eur. Spine J.* **2001**, *10*, S86−S95.

(17) Wopenka, B.; Pasteris, J. D. A Mineralogical Perspective on the Apatite in Bone. *Mater. Sci. Eng., C* **2005**, *25*, 131−143.

(18) Frisch, M. J.; Trucks, G. W.; Schlegel, H. B.; Scuseria, G. E.; Robb, M. A.; Cheeseman, J. R.; Scalmani, G.; Barone, V.; Mennucci, B.; Petersson, G. A.; Nakatsuji, H.; Caricato, M.; Li, X.; Hratchian, H. P.; Izmaylov, A. F.; Bloino, J.; Zheng, G.; Sonnenberg, J. L.; Hada, M.; Ehara, M.; Toyota, K.; Fukuda, R.; Hasegawa, J.; Ishida, M.; Nakajima, T.; Honda, Y.; Kitao, O.; Nakai, H.; Vreven, T.; Montgomery, J. A.; Peralta, J. E.; Ogliaro, F.; Bearpark, M.; Heyd, J. J.; Brothers, E.; Kudin, K. N.; Staroverov, V. N.; Keith, T.; Kobayashi, R.; Normand, J.; Raghavachari, K.; Rendell, A.; Burant, J. C.; Iyengar, S. S.; Tomasi, J.; Cossi, M.; Rega, N.; Millam, J. M.; Klene, M.; Knox, J. E.; Cross, J. B.; Bakken, V.; Adamo, C.; Jaramillo, J.; Gomperts, R.; Stratmann, R. E.; Yazyev, O.; Austin, A. J.; Cammi, R.; Pomelli, C.; Ochterski, J. W.; Martin, R. L.; Morokuma, K.; Zakrzewski, V. G.; Voth, G. A.; Salvador, P.; Dannenberg, J. J.; Dapprich, S.; Daniels, A. D.; Farkas, O.; Foresman, J. B.; Ortiz, J. V.; Cioslowski, J.; Fox, D. J. *Gaussian 09*; Gaussian, 2010.

(19) Becke, A. D. Density-functional thermochemistry. III. The role of exact exchange. *J. Chem. Phys.* **1993**, *98*, 5648.

(20) Mahmood, T.; Saddique, M. T.; Naeem, A.; Westerhoff, P.; Mustafa, S.; Alum, A. Comparison of Different Methods for the Point of Zero Charge Determination of NiO. *Ind. Eng. Chem. Res.* **2011**, *50*, 10017−10023.

(21) García, V.; Moreno-Piraján, J. C.; Giraldo, L. Construcción de un Calorímetro para la Determinación de Entalpías de Inmersión. *Inf. Tecnol.* **2007**, *18*, 59−70.

(22) Knuuttila, P.; Knuuttila, H.; Nishida, T.; Enzell, C. R.; Åkeson, Å.; Lundquist, G. The Crystal and Molecular Structure of N-(Phosphonomethyl)Glycine (Glyphosate). *Acta Chem. Scand.* **1979**, *33b*, 623−626.

(23) Öztürk Kiraz, A.; Kaya, S.; Gök, C. Structural and Electronic Properties of Nano Hydroxyapatite. *Acta Phys. Pol., A* **2020**, *137*, 1017−1022.

(24) Mandeep; Gulati, A.; Kakkar, R. DFT Study of Adsorption of Glyphosate Pesticide on Pt-Cu Decorated Pyridine-like Nitrogen-Doped Graphene. *J. Nanoparticle Res.* **2020**, *22*, 1−15.

(25) Seyed Khademi, S. M.; Telgheder, U.; Valadbeigi, Y.; Ilbeigi, V.; Tabrizchi, M. Direct Detection of Glyphosate in Drinking Water Using Corona-Discharge Ion Mobility Spectrometry: A Theoretical and Experimental Study. *Int. J. Mass Spectrom.* **2019**, *442*, 29−34.

(26) Lima, J. D. M.; Gomes, D. S.; Frazão, N. F.; Soares, D. J. B.; Sarmento, R. G. Glyphosate adsorption on C60 fullerene in aqueous medium for water reservoir depollution. *J. Mol. Model.* **2020**, *26*, 110.

(27) Guo, F.; Zhou, M.; Xu, J.; Fein, J. B.; Yu, Q.; Wang, Y.; Huang, Q.; Rong, X. Glyphosate Adsorption onto Kaolinite and Kaolinite-Humic Acid Composites: Experimental and Molecular Dynamics Studies. *Chemosphere* **2021**, *263*, 127979.

(28) Wang, M.; Liu, Y.; Yao, Y.; Han, L.; Liu, X. Comparative Evaluation of Bone Chars Derived from Bovine Parts: Physicochemical Properties and Copper Sorption Behavior. *Sci. Total Environ.* **2020**, *700*, 134470.

(29) Alkurdi, S. S. A.; Al-Juboori, R. A.; Bundschuh, J.; Bowtell, L.; McKnight, S. Effect of Pyrolysis Conditions on Bone Char Characterization and Its Ability for Arsenic and Fluoride Removal. *Environ. Pollut.* **2020**, *262*, 114221.

(30) Tomasini, E.; Siracusano, G.; Maier, M. S. Spectroscopic, Morphological and Chemical Characterization of Historic Pigments Based on Carbon. Paths for the Identification of an Artistic Pigment. *Microchem. J.* **2012**, *102*, 28−37.

(31) Khan, A. F.; Awais, M.; Khan, A. S.; Tabassum, S.; Chaudhry, A. A.; Rehman, I. U. Raman Spectroscopy of Natural Bone and Synthetic Apatites. *Appl. Spectrosc. Rev.* **2013**, *48*, 329−355.

(32) Castillo-Paz, A. M.; Londoño-Restrepo, S. M.; Tirado-Mejía, L.; Mondragón, M. A.; Rodríguez-García, M. E. Nano to Micro Size Transition of Hydroxyapatite in Porcine Bone during Heat Treatment with Low Heating Rates. *Prog. Nat. Sci.: Mater. Int.* **2020**, *30*, 494−501.

(33) Mohd Pu'ad, N. A. S.; Koshy, P.; Abdullah, H. Z.; Idris, M. I.; Lee, T. C. Syntheses of Hydroxyapatite from Natural Sources. *Heliyon* **2019**, *5*, No. e01588.

(34) Thommes, M.; Kaneko, K.; Neimark, A. V.; Olivier, J. P.; Rodriguez-Reinoso, F.; Rouquerol, J.; Sing, K. S. W. Physisorption of gases, with special reference to the evaluation of surface area and pore size distribution (IUPAC Technical Report). *Pure Appl. Chem* **2015**, *87*, 1051 aop.

(35) Sasaki, K.; Tsuruyama, S.; Moriyama, S.; Handley-Sidhu, S.; Renshaw, J. C.; Macaskie, L. E. Ion Exchange Capacity of Sr2+ onto Calcined Biological Hydroxyapatite and Implications for Use in Permeable Reactive Barriers. *Mater. Trans.* **2012**, *53*, 1267−1272.

(36) Rojas-Mayorga, C. K.; Silvestre-Albero, J.; Aguayo-Villarreal, I. A.; Mendoza-Castillo, D. I.; Bonilla-Petriciolet, A. A New Synthesis Route for Bone Chars Using CO2 Atmosphere and Their Application as Fluoride Adsorbents. *Microporous Mesoporous Mater.* **2015**, *209*, 38−44.

(37) Mendes, K. F.; de Sousa, R. N.; Takeshita, V.; Alonso, F. G.; Régo, A. P. J.; Tornisielo, V. L. Cow Bone Char as a Sorbent to Increase Sorption and Decrease Mobility of Hexazinone, Metribuzin, and Quinclorac in Soil. *Geoderma* **2019**, *343*, 40−49.

(38) Haberko, K.; Bućko, M. M.; Mozgawa, W.; Pyda, A.; Brzezińska-Miecznik, J.; Carpentier, J. Behaviour of Bone Origin Hydroxyapatite at Elevated Temperatures and in O2 and CO2 Atmospheres. *Ceram. Int.* **2009**, *35*, 2537−2540.

(39) Giraldo, L.; Rodríguez-Estupiñán, P.; Moreno-Piraján, J. C. Calorimetry of Immersion in the Energetic Characterization of Porous Solids. *Calorimetry—Design, Theory and Applications in Porous Solids*; InTech, 2018.

(40) Tihan, T. G.; Ionita, M. D.; Popescu, R. G.; Iordachescu, D. Effect of hydrophilic-hydrophobic balance on biocompatibility of poly(methyl methacrylate) (PMMA)-hydroxyapatite (HA) composites. *Mater. Chem. Phys.* **2009**, *118*, 265−269.

(41) Skwarek, E.; Goncharuk, O. V.; Janusz, W.; Pakhlov, E. M.; Gun'ko, V. M. Heats of Immersion of Hydroxyapatite and Hydroxyapatite/Fumed Oxides Composites in Water and n-Decane. *Mater. Chem. Phys.* **2018**, *215*, 99−103.

(42) Dorozhkin, S. V. Dissolution Mechanism of Calcium Apatites in Acids: A Review of Literature. *World J. Methodol.* **2012**, *2*, 1−17.

(43) Margolis, H. C.; Moreno, E. C. Kinetics of Hydroxyapatite Dissolution in Acetic, Lactic, and Phosphoric Acid Solutions. *Calcif. Tissue Int.* **1992**, *50*, 137−143.

(44) wu, M.-S.; Higuchi, W. I.; Fox, J. L.; Friedman, M. Kinetics and Mechanism of Hydroxyapatite Crystal Dissolution in Weak Acid Buffers Using the Rotating Disk Method. *J. Dent. Res.* **1976**, *55*, 496−505.

(45) Thomann, J. M.; Voegel, J. C.; Gramain, P. Kinetics of Dissolution of Calcium Hydroxyapatite Powder. III: PH and Sample Conditioning Effects. *Calcif. Tissue Int.* **1990**, *46*, 121−129.

(46) Ardhaoui, K.; Ben Cherifa, A.; Jemal, M. Calcium Hydroxyapatite Solubilisation in the Hydrochloric and Perchloric Acids. *J. Therm. Anal. Calorim.* **2005**, *81*, 251−254.

(47) Defarge, N.; Spiroux de Vendômois, J.; Séralini, G. E. Toxicity of Formulants and Heavy Metals in Glyphosate-Based Herbicides and Other Pesticides. *Toxicol. Rep.* **2018**, *5*, 156−163.

(48) Sen, K.; Datta, J. K.; Mondal, N. K. Box-Behnken optimization of glyphosate adsorption on to biofabricated calcium hydroxyapatite: kinetic, isotherm, thermodynamic studies. *Appl. Nanosci.* **2021**, *11*, 687−697.

(49) Pan, H.; Tao, J.; Xu, X.; Tang, R. Adsorption Processes of Gly and Glu Amino Acids on Hydroxyapatite Surfaces at the Atomic Level. *Langmuir* **2007**, *23*, 8972−8981.

(50) El Rhilassi, A.; Mourabet, M.; Bennani-Ziatni, M.; El Hamri, R.; Taitai, A. Interaction of Some Essential Amino Acids with Synthesized Poorly Crystalline Hydroxyapatite. *J. Saudi Chem. Soc.* **2016**, *20*, S632−S640.

(51) Hoff, S. E.; Liu, J.; Heinz, H. Binding Mechanism and Binding Free Energy of Amino Acids and Citrate to Hydroxyapatite Surfaces as a Function of Crystallographic Facet, PH, and Electrolytes. *J. Colloid Interface Sci.* **2022**, *605*, 685−700.